ELSEVIER

Contents lists available at ScienceDirect

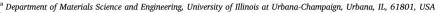
Materials Science & Engineering A

journal homepage: http://www.elsevier.com/locate/msea



A microscale additive manufacturing approach for in situ nanomechanics

S. Daryadel ^a, A. Behroozfar ^b, M. Minary-Jolandan ^{b,*}



b Department of Mechanical Engineering, The University of Texas at Dallas, Richardson, TX, 75080, USA



Keywords:
In situ nanomechanics
Micro-pillar compression
Micro-scale additive manufacturing (AM)
Metals and alloys

ABSTRACT

In situ nanomechanics in scanning electron microscope (SEM) and transmission electron microscope (TEM) has been the gold-standard for direct observation of deformation mechanisms of metals and alloys. The extracted deformation mechanisms complement the process – microstructure – property relationship that is required for the full understanding of the mechanical behavior of these materials. Micro-pillar compression is perhaps the most frequently used method for such studies. Fabrication of micro-pillars from bulk materials relies on milling by the focused ion beam (FIB), which often requires several tens of hours of the equipment time, and the associated expenses. Additionally, the heavy ion bombardment by FIB may introduce damage into materials, which in turn may result in compromised interpretation of materials' behavior. We introduce a microscale additive manufacturing (AM) approach that enables direct deposition of nano-pillars and micro-pillars of metals and alloys in room environment. In addition to the size, this process allows control over the microstructure of the deposited metals and alloys. Depending on the size and microstructure, a typical micro-pillar can be fabricated in a few minutes to tens of minutes at very low cost and without any beam-induced damages. When combined with in situ instrumentation, this approach may enable high-throughput investigation of the process – microstructure – property relationship, in particular for nano-crystalline and nano-twinned metals and alloys.

1. Introduction

There is a constant demand for development of high-performance metals and alloys with enhanced strength at a lower weight. Development of metals and alloys with new microstructure and/or composition often requires knowledge on the process - microstructure - property relationship. In particular, to understand the effect of the microstructure on mechanical properties, various experimental methods such as simple tension, three-point bending, and fracture toughness tests are used. Often times, knowledge on the deformation mechanism at the micro and nanoscale is required to complement the bulk mechanical properties [1]. In situ scanning electron microscope (SEM) and transmission electron microscope (TEM) experiments have provided powerful characterization methods for the direct observation of deformation mechanisms [2–9]. In particular, in situ SEM micro-pillar compression has been the hallmark of nanomechanical characterization techniques [10-20]. In this experiment, pillars with diameters of several microns or sub-micron are compressed using a flat microscale tip; meanwhile, the deformation of the pillar is captured in a series of SEM images. The obtained SEM micrographs are analyzed combined with

force-deformation responses to construct the deformation mechanism of the material.

To obtain the micro-pillars for *in situ* SEM micro-compression experiments, often thin films or bulk of the material of interest are milled using focused ion beam (FIB) in consecutive steps in a top-down approach. A typical micro-pillar may require FIB time of few hours to more than 24 h [10,13], which can mount to hundreds to a few thousands of dollars for sample preparations, considering the high cost of FIB. The long duration exposure to heavy ions in FIB can also introduce damage into the material [13,21–23]. Ions from the beam may also get embedded into the material of the micro-pillar in this process. It has been shown that the composition and microstructure of the surface layer of the material can be compromised in the FIB milling process. This in turn, may alter the true deformation mechanism in the material and lead to compromised conclusions. Moreover, there are practical difficulties with fabricating accurate pillars with a diameter of less than 0.5 μ m [10, 12]

An alternate nanofabrication method has also been reported based on electroplating into a PMMA (Poly(methyl methacrylate)) template that is patterned by electron beam lithography [24]. The developed

E-mail address: majid.minary@utdallas.edu (M. Minary-Jolandan).

^{*} Corresponding author.

technique is a nondamaging method to fabricate isolated metal nanopillars with a diameter of less than $100\,\mathrm{nm}$ for mechanical characterization. While this method is efficient for rapid fabrication of arrays of nanopillars, it requires additional processes for template fabrication .

We introduce a bottom-up process, termed localized pulsed electrodeposition (L-PED), based on microscale AM to enable a more convenient method for in situ SEM studies of mechanical properties and deformation mechanisms of metals and alloys. This process enables direct deposition of nano-pillars and micro-pillars of metals and alloys in room environment. In addition to the size, this process enables control over the microstructure of the deposited material to facilitate investigation of microstructure - property relationship. Depending on the size and type of the desired microstructure, a typical micro-pillar can be fabricated in a single step in a few minutes to tens of minutes at a low cost and without any beam-induced damage. When combined with in situ instrumentation, this approach may enable high-throughput investigation of the process - microstructure - property relationship in particular for nano-crystalline and nano-twinned metals and alloys. In Fig. 1, this microscale AM process is schematically compared to the FIB milling and template-based electrodeposition approaches for fabrication of micro-pillars for in situ SEM studies.

2. Materials and methods

Direct printing of Cu micro-pillars was carried out using glass micropipettes that were pulled to the desired pillar diameter using a pipette puller (Model P-97, Sutter Instrument). Solution of CuSO₄ (100 mM) and H₂SO₄ (1 M) was utilized as the plating electrolyte. A substrate of gold-coated silicon and a copper wire inserted from the back of the nozzle functioned as the working electrode and the counter electrode, respectively. The electrical potential between the two electrodes was controlled by a potentiostat/galvanostat (VersaSTAT 4, Princeton Applied Research). The relative position of the nozzle and substrate and printing procedure was handled by two high-resolution three-axis positioning linear stages (Newport, Inc.). The RH of the printing environment was controlled during the process using a humidifier and a remote hygrometer. The printing procedure was monitored *in situ* by an objective optical lens coupled with a CCD camera (XM-10, Olympus).

The morphology and geometry of the micro-pillars were investigated

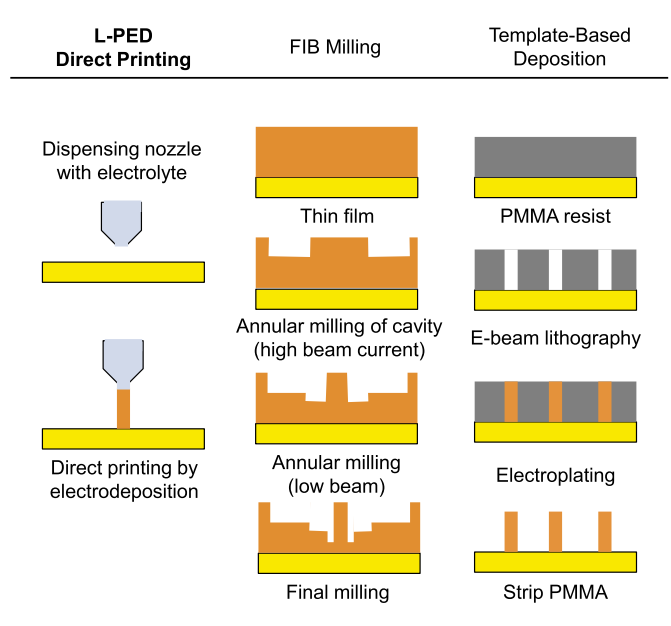


Fig. 1. Comparison of the L-PED AM process with the FIB milling and template-based electroplating approaches for fabrication of micro-scale pillars. AM enables fabrication of specimens in a single step at low cost in room environment.

using an SEM (Supra 40 Zeiss). High-resolution FIB imaging (FEI Nova Nanolab 200) was utilized to study the microstructure of the printed Cu. The cross-section of the micro-pillar was milled at a final acceleration voltage of 30 keV and a current of 10 pA and observed with the same parameters. Micro-compression experiments were carried out on the printed micro-pillars using an in situ SEM nanoindentation system (NanoFlip, Nanomechanics). A 50 μm diameter flat punch tip was used as the compression anvil. The tests were run at displacement-control mode at a constant displacement rate (constant strain rate of $1\times 10^{-3}~\rm s^{-1}$). The true stress-strain response was calculated based on the obtained load – displacement data, and the geometry of each specimen. The electrical characterization of individual pillars was performed in situ SEM using a nanomanipulator (Kleindiek Nanotechnik), a power supply, and a picoammeter (Keithley). Three samples were tested for each characterization type.

3. Results and discussion

3.1. Description of the L-PED process

The new approach for AM of metallic micro-pillars for in situ SEM micro-compression experiments is based on 3D printing via localized electrodeposition (Fig. 2A) [25,26]. This process is based on the concept of confining the electrodeposition process to a small area at the tip of a nozzle. Consider a nozzle (often a glass capillary) filled with an electrolyte of the metal of interest, as an example electrolyte of CuSO₄ for the printing Cu structures. The nozzle is steered in 3D-XYZ by a set of precision motorized stages or piezoelectric actuators, which are controlled by a computer program. The input to the program is a CAD model of the desired geometry to be fabricated, which in this case will be a straight micro-pillar. When the nozzle approaches to a conductive substrate, a meniscus (or also known as liquid bridge) forms between the tip of the nozzle and the substrate. This liquid bridge between the tip of the nozzle and the substrate forms the electrolyte bath for the localized electrodeposition process, and it moves with the nozzle in 3D-XYZ as the material is being deposited. A potentiostat applies the desired potential between the anode inserted in the nozzle and the cathode (substrate). Metal ions from the electrolyte reduce at the growth front within the electrolyte meniscus, and through the controlled relative motion of the nozzle and the substrate, metal is printed in any desired 3D geometry (Fig. 2B). A thin metal film is deposited on a Si (silicon) substrate to function as the cathode.

It's noteworthy that the initial distance between the nozzle tip and the substrate to form the liquid bridge depends on different factors including the surface condition, which comes from the nature of the solution and the nozzle, and the diameter of the tip. In this study, the formation of the meniscus is perceived by real-time monitoring of the current profile in the circuit during the process. In approaching step, an appropriate low potential $(-0.02\ V)$ is applied between the electrodes. A sharp rise in the current indicates liquid bridge formation between the nozzle tip and the substrate. The approach potential is chosen low to not deposit any metal in this step.

3.2. Process parameters of the L-PED manufacturing process

Potentiostatic vs. galvanostatic modes: In the electrodeposition process, the growth current is one of the critical parameters. Two modes of potentiostatic and galvanostatic can be employed to reduce the metal ions in this process. In the potentiostatic mode, the potential between the electrodes is controlled, while the current is measured as a dependent variable, while in the galvanostatic mode, the current between the electrodes is held constant using a current source, and the potential is measured as a function of time. In general, a three-electrode electrochemical cell is preferable in this process, because without a reference electrode the potentiostatic deposition can be problematic over time when the potential drop (*iR*-drop) through the electrolyte is high, and

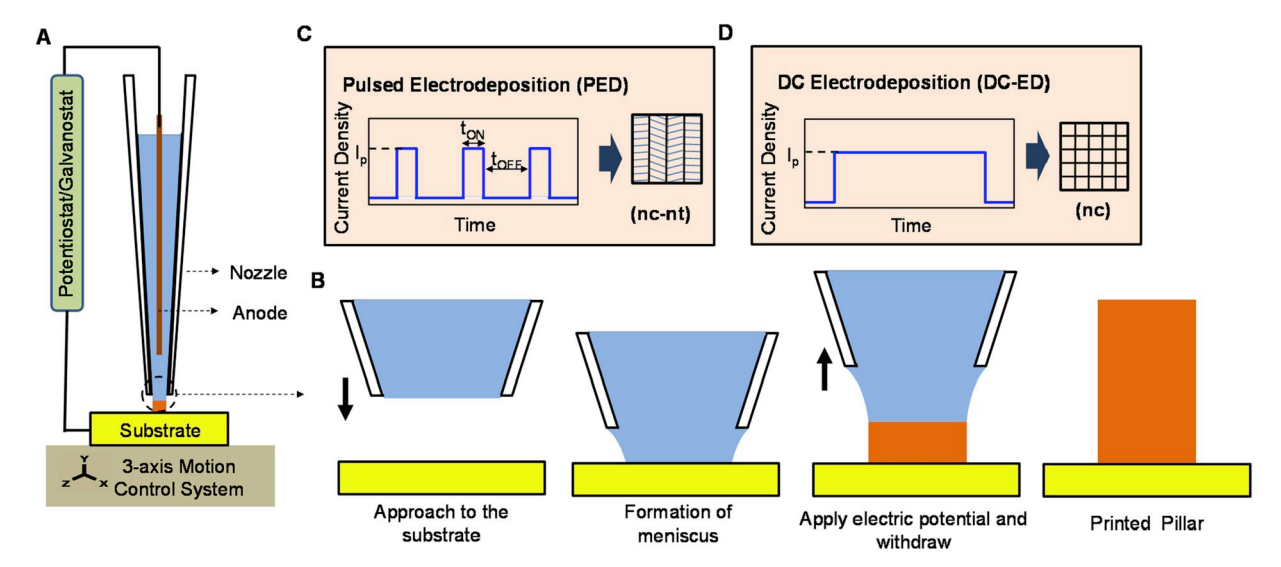


Fig. 2. (A) Schematic view of L-PED 3D printing setup. (B)–(C) Process parameters of the L-PED can be adjusted, and this enables control over the microstructure of the printed structures: (B) Pulsed electrodeposition (PED) results in nanocrystalline nanotwinned microstructure, while (C) DC electrodeposition (DC-ED) produces nanocrystalline microstructure. (D) The printing process of a micro-pillar using L-PED includes approach of the nozzle-tip to the substrate, formation of the meniscus (liquid bridge) between the tip and the conductive substrate as the confined electrodeposition bath, application of an electric potential between two electrodes and deposition of the metal ions at the growth front followed by controlled withdrawal motion of the nozzle.

when the counter electrode is polarized due to the application of high current density [27]. Currently, there is a limitation in adding a reference electrode in L-PED setup while using a nozzle with a small diameter. Therefore, the galvanostatic mode is desirable in L-PED as no feedback from the reference electrode (in the three-electrode systems) is required during the process, which makes the cell system for galvanostat much simpler than the potentiostat. Schematic of I-t curve for pulsed current in galvanostatic technique is depicted in Fig. 3A.

It is worth mentioning that in printing with nozzles less than 1 μm in

diameter, the iR-drop in the electrolyte is insignificant during the process (~mV range). Therefore, the potentiostatic mode with a two-electrode cell system can be used in this process with nozzles less than 1 μ m in diameter, while keeping the relative humidity (RH) of the environment constant. This is because having a very small area of the working electrode (nozzle tip) results in a very small current (nA range), regardless of the high resistance of the electrolyte due to small tip size of the nozzle (resistance in the $M\Omega$ range). Additionally, the counter electrode (or anode) does not get polarized because of the low current

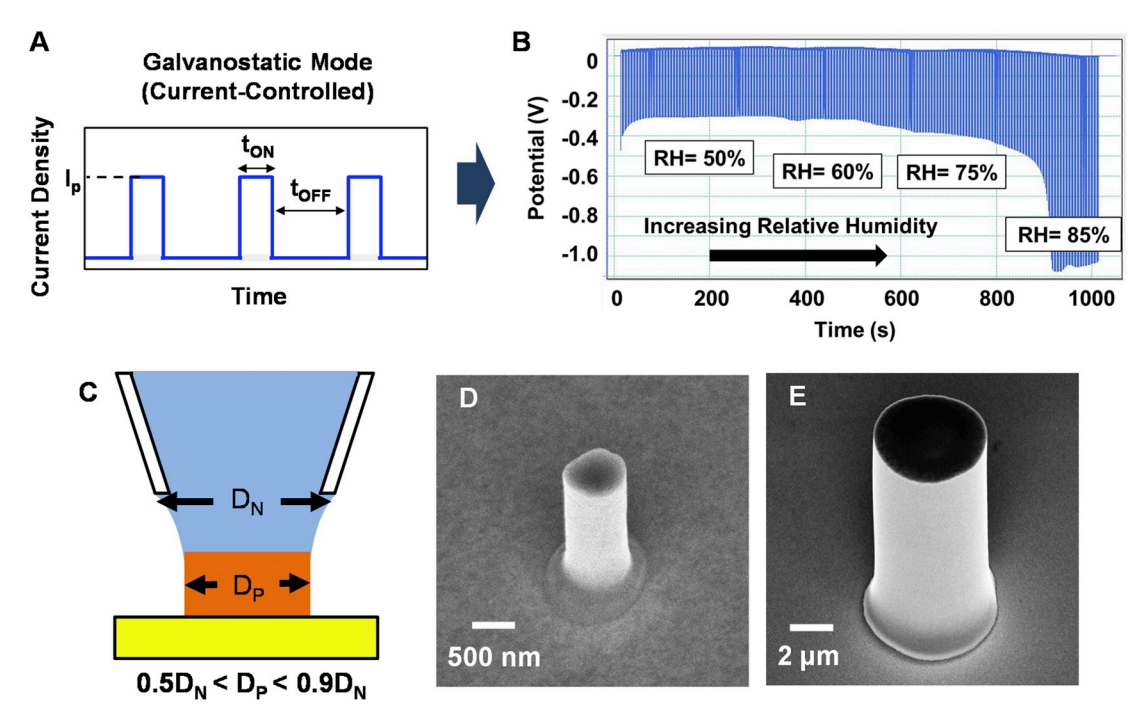


Fig. 3. (A) The schematic I-t (current-time) curve for the galvanostatic mode, where the current between the electrodes is controlled, and the potential is a dependent variable as a function of time. (B) Typical electric potential acquired during deposition of a micro-pillar in the galvanostatic mode while the RH increased. The potentiostat maintains the desired current during printing by varying the applied potential and compensates for the changes of the ionic flux due to changes of RH. (C) Dependence of the diameter of the printed pillar (D_P) on the nozzle tip diameter (D_N) . Micro-pillars with a diameter in the range of 0.5- to 0.9-time of the diameter of the nozzle can be printed. (D)–(E) Cu micro-pillars printed using L-PED process with different diameters of 0.73 μ m and 5.25 μ m by different nozzles.

density resulting from the large surface area of the anode (the surface area of the wire inside the pipette) compared to the working electrode (on the order of the area of the nozzle tip).

The evaporation rate is one of the key factors in L-PED process [28]. During printing in the potentiostatic mode, the RH of the environment needs to be kept constant, because altering it results in a change of ionic flux toward the cathode and change of the concentration of the ions at the cathode surface, and consequently change of the growth rate of the metal. However, in the galvanostatic mode, by maintaining the RH in the range 45–85%, one can 3D print with a constant deposition rate throughout the process. During printing, the system adjusts applied potential, which compensates for the change of ionic flux due to variation in the evaporation rate, and keeps the current and growth rate steady during printing (Fig. 3B). Therefore, the process is less dependent on the RH of the environment and evaporation of the electrolyte in the galvanostatic mode.

Size of the printed pillars: The size of the printed pillars depends on the size of the electrolyte meniscus between the tip of the nozzle and the growth front (initially the substrate). Based on the theoretical models of the liquid capillary, the diameter and height of the meniscus are on the order of the magnitude of the nozzle tip, which can vary from sub-100 nm to several millimeters, based on the size of the desired pillar to be fabricated. Often, a glass pipette puller is used for fabrication of nozzles with the desired diameter.

The multi-physics models and experimental results have shown that for a given nozzle diameter, pillars in the range of 0.5- to 0.9-time of the diameter of the nozzle can be 3D printed (Fig. 3C) [29]. This is because increasing the withdrawal speed of the nozzle stretches the electrolyte liquid bridge within its stable range and results in a finer diameter pillar for a given tip diameter of the nozzle. Therefore, the size of the printed pillars can be controlled by adjusting the withdrawal speed of the nozzle depends on the deposition rate of the pillars, which depends on the deposition parameters such as the concentration of the electrolyte, the RH of the environment, and the applied potential. Fig. 3D and E show two different Cu micro-pillars with a diameter of 0.73 μm and 5.25 μm printed using L-PED method by two different nozzles.

The height of the pillars that can be fabricated is only limited by the travel range of the piezo actuator. For *in situ* SEM micro-compression experiments, micro-pillars are preferred to have a specific aspect ratio (generally 2:1 to 3:1 height-to-diameter) to ensure that they are not too short to be affected by the top and bottom constraints, and not too tall to buckle during the micro-compression experiment. In this study, the sample length-to-diameter aspect ratio was kept at \sim 2.5:1 to minimize the effects of buckling and the other artifacts. Considering the geometry of the micro-pillars, the critical load which they can bear without buckling can be calculated using the Euler's critical load equation. The measured critical load to avoid buckling was calculated to be \sim 49 mN, while the maximum load applied during micro-compression tests was \sim 12 mN.

Microstructure control: The L-PED process is capable of control over the microstructure of the printed pillars, to the extent of microstructure control in the bulk electrodeposition process. Specifically, in electrodeposition, the grain size, grain orientation, and nanotwin density and orientation can be controlled through process parameters. This capability may enable investigation of the process - microstructure - property relationship of different materials. The deposition parameters can be controlled during the printing process at different modes of direct current electrodeposition (DC-ED) or pulsed current electrodeposition (PED) with arbitrary current densities and duty cycles. As demonstrated schematically in Fig. 2C and D, the DC-ED process results in nanocrystalline (nc) microstructure, while the introduction of the OFF-time during the PED changes the microstructure of the printed metal to nanocrystalline nanotwinned (nc-nt) microstructure with columnarshaped grains [26]. The process can be extended to control over the grain size and orientation, the density and orientation of twins by

adjusting the deposition parameters. The effect of the L-PED electrochemical process parameters on the density and the orientation of the twin boundaries and grain size were investigated in Ref. [30]. For instance, in the electrodeposition of nt-Cu, increasing the average current density and accordingly, the deposition rate of nt-Cu, increases the twin density [30]. In particular, increasing the peak current density increases the twin density significantly while decreasing the grain size. Rising the pulse ON-time period during printing process increases the density of TBs and their alignment within the grains by increasing the average current density. Additionally, increasing the OFF-time period increases the grain size while decreasing the twin density [30]. FIB and TEM imaging is often employed to investigate the microstructure of the pillars. The FIB ion-contrast image of the cross-section of the pillar provides a primary qualitative knowledge on the microstructure, and TEM can deliver the details at higher resolution.

Deposition rate: One advantage of the L-PED is high throughput fabrication of the micro-pillars compared to the FIB-based milling process. The printing speed of the micro-pillars depends on the deposition mode and the process parameters for specific microstructure. Generally, the higher average deposition rate is achieved in DC-ED mode where there is no interruption in growth during printing ($T_{OFF} = 0$). However, in order to get various microstructures, in particular, twin boundaries (TBs) within the grains, the OFF-time is introduced periodically to interrupt the growth, which significantly lowers the printing speed. For

instance, introducing OFF-time with a duty cycle of 1/100 $\left(\frac{T_{ON}}{T_{ON} + T_{OFF}}\right)$

while keeping the ON-current density constant, results in 100 times reduction in the printing rate. Based on our experiments, using different deposition modes and parameters including the applied current density and duty cycle, Cu micro-pillar with the printing rate in the range of 2 nm/s to 250 nm/s depending on the desired microstructure can be fabricated. For example, fabrication of a typical nc-Cu micro-pillar with 5 μm diameter and 15 μm height at an average deposition rate of 100 nm/s takes about 2.5 min. As a comparison, fabrication of the same pillar with FIB milling would take more than 4 h of ion milling, which, in addition to the prohibitive cost, may leave the sample with damaged microstructure.

It's noteworthy that the FIB milling approach has certain advantages for preparation of micro-pillars for in situ SEM micro-compression experiments. FIB can operate on almost all types of metals and alloys while the AM method discussed here can be applied to a subset of metals and alloys that can be electrodeposited. So far, the L-PED has been implemented successfully for additive manufacturing of copper, nickel, platinum, silver, nickel alloys, and conductive polymers. Additionally, the deposition rate of the pillars is highly dependent on the electrolyte concentration. Increasing the concentration of Cu ions in the electrolyte increases the current density during the ON-time and accordingly increases the deposition rate. Due to the fast evaporation of water in L-PED process, the concentration of metal ions in the meniscus varies from the bulk concentration and increases during the OFF-time. Therefore, there is a limitation for increasing the concentration because in the nozzles with smaller diameter, which the volumetric evaporation rate is higher, this will cause clogging of the tip. It should be noted that during the ONtime period, the concentration of ions decreases due to ion consumption. The detailed status of the electrolyte concentration during the process is discussed in multi-physics simulation studies presented in our recent publications [25].

3.3. In situ characterization

Microstructure characterization: Fig. 4A shows an SEM image of an array of directly printed Cu micro-pillars using the L-PED process with a diameter distribution of $4.60 \pm 0.08 \, \mu m$ and height of $11.80 \pm 0.11 \, \mu m$. The micro-pillars were printed with T_{on} of 20 ms, T_{off} of 2 s. The peak current density during deposition was $\sim 3.7 \, \text{A/cm}^2$ at a deposition rate of 12 nm/s. The printing of each micro-pillar took about $\sim 16 \, \text{min}$, at this

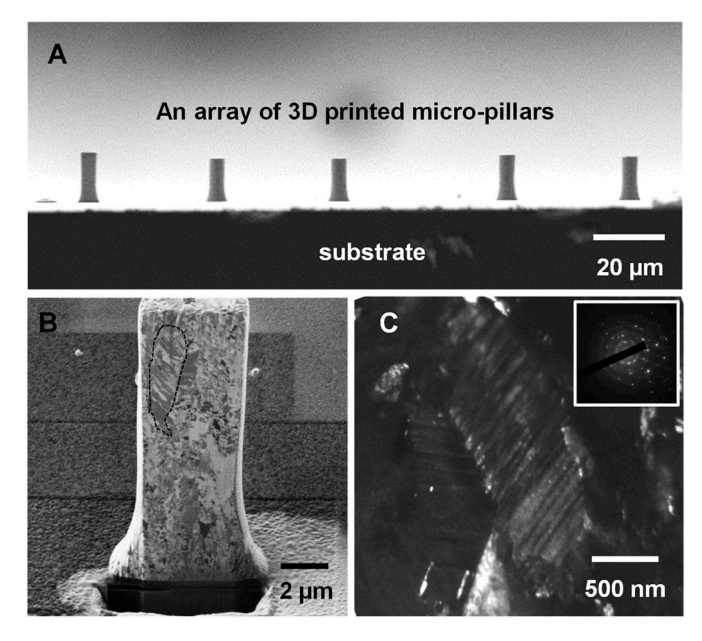


Fig. 4. (A) An SEM image of an array of directly printed Cu micro-pillars using the L-PED process with a diameter distribution of $4.6\pm0.08\,\mu m$. The micropillars were printed with T_{on} of 20 ms, T_{off} of 2 s and the peak current density of 3.74 ± 0.17 A/cm² at a deposition rate of $12\,n m/s$. The printing of each micro-pillar took about ~16 min. (B) The micro-pillar was sectioned using FIB to reveal its internal structure. The deposited material is fully dense with no apparent porosity. The ion-channeling contrast image reveals the microstructure of the printed metal, including the grain size and shape and existence of the twin boundaries. One of the columnar-shaped grains is delineated by a dashed line. (C) The TEM image of the pillar printed by the L-PED process shows a typical nanotwinned grain with the corresponding diffraction pattern (inset), which reveals the nanocrystalline structure.

deposition rate, which is much faster compared to the FIB milling process. The pillar was sectioned using FIB to reveal its internal structure (Fig. 4B). It can be observed that the pillar is fully dense with no

apparent porosity. Fig. 4B presents the FIB ion channel contrast image of the cross-section of a micro-pillar printed using L-PED process. The result exhibited ultrafine-grained microstructure, and the channeling contrast revealed the existence of TBs within some of the grains. As can be seen, the introduction of the OFF-time in the L-PED process changes the microstructure of the printed metal similar to the bulk PE process.

The L-PED deposited pillars demonstrated nanotwinned grains with an average diameter of $\sim\!300\,\mathrm{nm}$, separated into twin/matrix lamellar structures by TBs. The average grain size was measured using the FIB cross-section image and intercept procedure. Fig. 4C shows the TEM image of the cross-section of a micro-pillar. The inset diffraction pattern reveals the polycrystalline structure of the micro-pillar. A grain with TBs is highlighted in the image. It is noteworthy that more detailed high-resolution TEM images and microstructural analysis from the printed structures are presented in our recent publications where the formation of nt-metallic microstructures was established [25,26].

Mechanical characterization: Mechanical properties of the micropillars printed by the L-PED process were characterized using in situ SEM micro-compression experiments using a nanoindenter with a specialized punch. Fig. 5A and B shows photographs of the nanoindenter and the substrate containing the 3D printed micro-pillars in situ SEM. A conductive flat punch tip was employed as the compression anvil. The conductive tip is required for in situ SEM experiments to avoid charging of the indenter tip by the electron beam. Experiments can be carried out under both load-control and displacement-control modes. It's noteworthy that nanoindenter is intrinsically a load-controlled system, however, a constant displacement rate can be achieved by a feedback control loop. Fig. 5C shows in situ SEM micro-compression experiment on an individual micro-pillar from an array of 3D printed pillars using a conductive diamond flat punch tip with a diameter of 50 µm. In practice, such experiments can be automated for a large array of micro-pillars precisely 3D printed using the described AM process in regular distances.

A representative stress-strain response from one of the micro-pillars is shown in Fig. 5D. The stress-strain response of each micro-pillar was calculated from the obtained load and displacement data, and the geometry of the micro-pillar. The true stress-strain was calculated based on

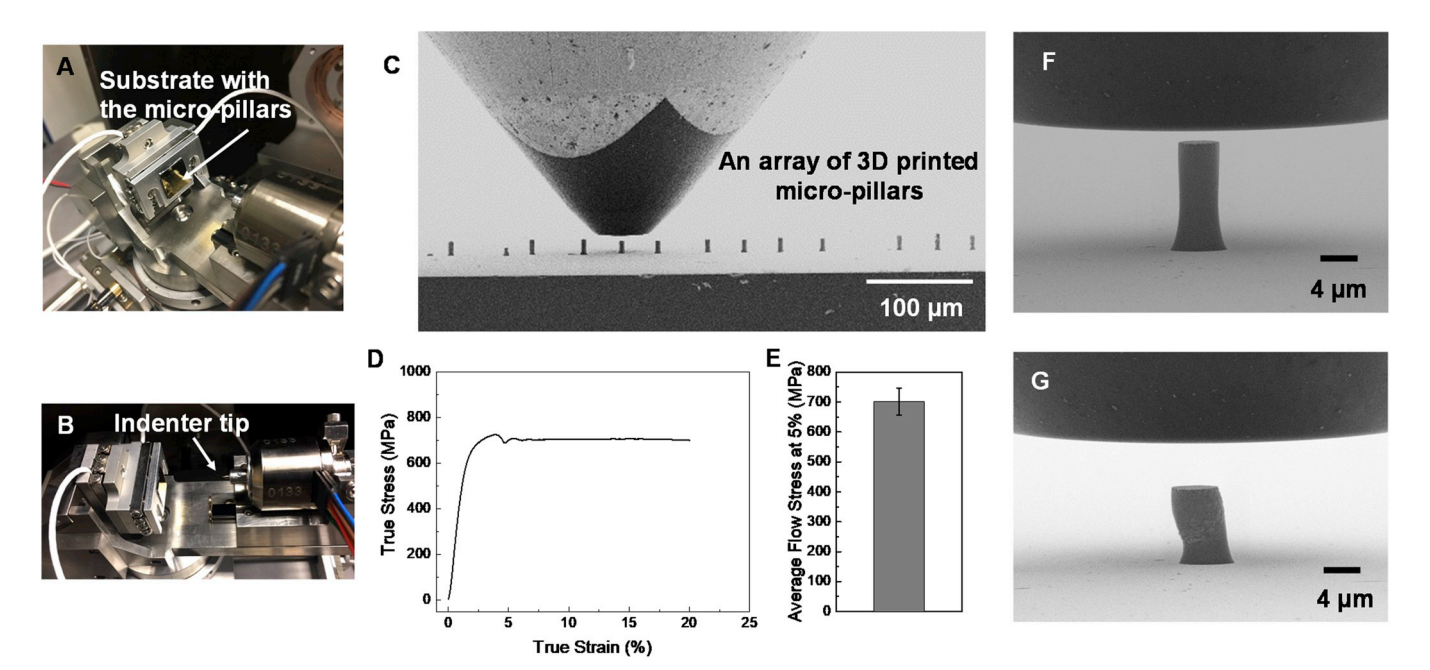


Fig. 5. (A)–(B) Photographs of the nanoindenter and the substrate containing the 3D printed micro-pillars *in situ* SEM. (C) Micro-compression experiment *in situ* SEM on individual micro-pillars from an array of 3D printed pillars using a flat punch tip. (D) A typical stress-strain response of nc-nt Cu (nanocrystalline-nanotwinned copper) micro-pillar printed using the L-PED process. (E) The average flow stress of the pillars at a strain of 5%. (F)–(G) SEM images of the micro-pillar pre- and post-compression, respectively.

the assumption of constant volume for the pillars during the experiments. The pillars exhibited near-perfect elasto-plastic behavior with no clear hardening and smooth flow stress. Because of the small size of grains and the presence of twin boundaries (TBs) in the printed nc-nt Cu pillars, the activity of dislocations is reduced. Therefore, the material's response is near-perfect elastoplastic instead of work-hardened [31]. TBs by acting as barriers to dislocations prevent rapid deformation process in nc-nt samples. Fig. 5D illustrates the average flow stress at 5% strain for the printed pillars. The flow stress is reported at 5% strain due to the fact that the yield point was not clear in such small-scale testing . The result indicates an average flow stress of 701 \pm 45 MPa for the nc-nt Cu pillars, which agrees with previously reported strength for such microstructure [32]. In nc-nt Cu micro-pillars, the twin boundaries block the motion of dislocations, giving rise to such remarkable flow stress. This is remarkable given that such micro-pillar was fabricated with an AM process. It is noteworthy to mention that the measured slope of the elastic region obtained from the stress-strain curve is lower than the expected value for the copper's Young's modulus. This discrepancy in micro-compression experiments arises from the experimental artifacts and inaccuracy in the displacement measurement in the in situ nanomechanical testing during micro-pillar compression.

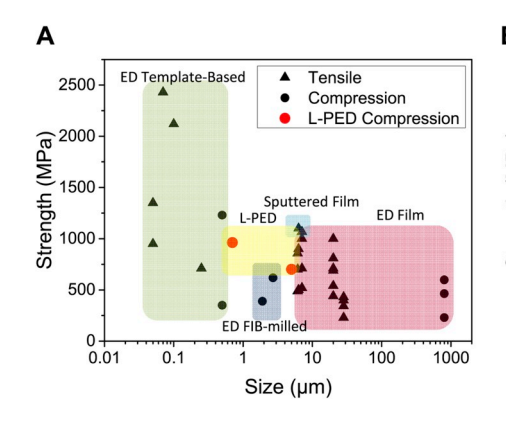
In situ SEM experiments enable real-time monitoring of the deformation of the material and its correlation with the stress-strain behavior. SEM images of the micro-pillar pre- and post-compression, respectively, are shown in Fig. 5F and G. The post-compression SEM image reveals localized plasticity in micro-pillar deformation, supporting that the failure is of a ductile nature. Additionally, it can be observed that the pillar after compression still holds a strong adhesion with the substrate. This is very important since a weak adhesion with the substrate may compromise obtained mechanical properties. The choice of proper substrate is essential to ensure such strong adhesion in the AM process.

There have been several experimental reports on the tension and compression properties of nt-Cu metals fabricated with different methods [32-41]. The strength of L-PED nc-nt Cu micropillars and other nt sample in the form of bulk solids, films, nanopillars or nanowires, is presented in Fig. 6A. All the reported nt structures exhibit high strength ranging from 230 MPa to 2400 MPa. The obtained range of strength for the printed structures by the L-PED process is consistent with the recent reports. L-PED pillars with a diameter of 4.6 μm and 0.7 μm exhibited average flow stress of 701 ± 45 MPa and 962 ± 26 MPa, respectively. The difference in the strength of various samples can be attributed to their specific deformation mechanism governed by their microstructure and dislocations behavior. It is known that different synthesis techniques and different parameters produce different kinds of microstructure [42], and the mechanical properties of nt materials are strongly influenced by the interaction of dislocations and TBs. Previous studies revealed that the TBs block the propagation of slip bands similar to that of the grain boundaries in acting as obstacles to strain propagation [42]. For instance, the strength of the nt-Cu increases with decreasing the twin thickness following the Hall-Petch relationship, similar to that of grain

refinement strengthening in nc metals, whereas samples with twin thickness of lower than 15 nm follow the inverse Hall-Petch relationship [38]. Also, studies showed that the perpendicular orientation of TBs with respect to the loading direction results in more strengthening, and samples with orthogonal TBs require additional applied stress to fail [35, 43]. It's noteworthy that other microstructural parameters, such as grain size and texture, affect the properties as well [42]. The process-microstructure-property relationship of the printed nt-Cu by the L-PED process was investigated to show how the electrochemical process parameters affect the mechanical properties of the printed metal [30]. In particular, an increase in the average current density resulted in a more aligned and higher density of TBs and enhancement of the strength of the printed metal [30].

Fig. 6B presents a more focused comparison of compression strength in L-PED nc-nt Cu micropillars and selected similar pillars fabricated with template-based electrodeposition and FIB milling. Interestingly, the strengths of L-PED samples are higher than those of their counterparts. In the template-based electrodeposited nanotwinned sample [33], grains are equiaxed with the TBs inclined to the grain boundaries, while in the L-PED fabricated pillars, most grains have the form of columns where the TBs are approximately perpendicular to the columnar axis. Therefore, the L-PED nanotwinned specimens, possessing a pronounced texture with <111> planes located preferentially parallel to the substrate, exhibit higher strength. The FIB-milled pillars [35] with near equivalent nanocrystalline microstructure and twin orientations, reveal slightly lower strength compared to the L-PED specimens. While this difference can be due to the slight dissimilarity in the microstructure of samples, it can also be attributed to the introduced damage into the material during the process. The results show that L-PED has the capability to fabricate pristine controlled microstructure with no initial dislocations, with comparable mechanical properties to the bulk sample [25,26].

Electrical characterization: The free-standing micro-pillar geometry is also attractive for characterization of electrical conductivity of the 3D printed material. The electrical conductivity of the 3D printed metal can also be used as an indirect method for probing the microstructure of the metal. We measured the electrical resistivity of the 3D printed micropillars in situ SEM by a nanomanipulator. The image of the experimental setup is shown in Fig. 7A. The conductive substrate on which the micro-pillars were deposited was used as the electric ground, while the tungsten probe was manipulated to measure the resistance of the pillar. The probing procedure is presented in Fig. 7B and C. First, we tightly pressed the probe on the top of the pillar to measure the total resistance (R_T) . The total resistance consists of the intrinsic resistance of the pillar (R_P) , the contact resistance, resistance of the circuitry, and resistance of the substrate (R_S) . The acquired total resistance is shown in Fig. 7D with the black line. Subsequently, the probe was placed on the bottom of the pillar to determine sum of the contact resistance, circuitry resistance, and substrate resistance (R_S), which is shown as the red line in Fig. 7D. Assuming the resistances are in series, the resistance of the pillar (R_p)



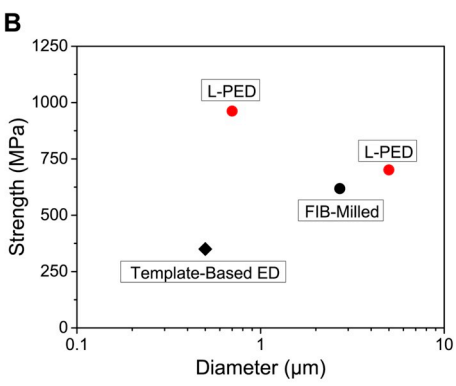


Fig. 6. (A) Comparison of the strength of nanotwinned copper L-PED micropillars (red symbols) and other reported nanotwinned sample in the form of electrodeposited or sputtered bulk solids and films, or nanopillars fabricated using FIB milling or template patterning [32–41]. (B) Comparison of compression strength in L-PED nc-nt Cu micropillars and similar pillars fabricated by the template-based electrodeposition and FIB milling with near equivalent nanocrystalline microstructure and twin orientations [33,35].[33,35]. (For interpretation of the references to colour in this figure legend, the reader is referred to the Web version of this article.)

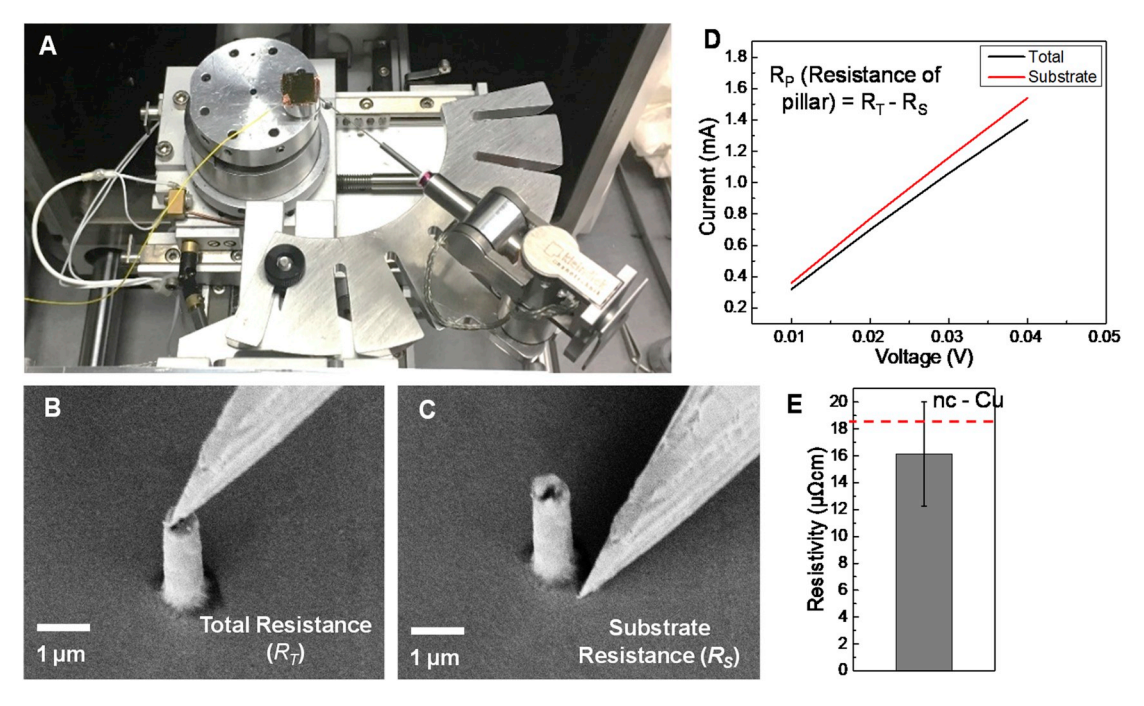


Fig. 7. (A) The *in situ* SEM setup for characterization of electrical properties of 3D printed micro-pillars. (B)–(C) SEM images of the procedure for measurement of the electrical resistivity of a pillar with a diameter of \sim 700 nm. (D) The typical I–V response on the top and bottom of a single 3D printed Cu micro-pillar. (E) The average calculated resistivity of the Cu micro-pillar. The red dash line demonstrates the resistivity of bulk nc-Cu at room temperature. (For interpretation of the references to colour in this figure legend, the reader is referred to the Web version of this article.)

was calculated by subtraction of R_S from R_T . Using the geometry of the micro-pillar obtained from the SEM images, the resistivity of the pillar can be calculated. $\rho = R \cdot A/L$, where R is the intrinsic resistance, A is the cross-sectional area, and L is the height of the micro-pillar. The result of the electrical characterization of nc-Cu pillars with an average diameter of \sim 700 nm is presented in Fig. 7E. The pillars exhibited an average resistivity of $16.14 \pm 3.90 \, \mu\Omega$.cm, which is close to the value for the bulk nc-Cu (red dash line) at room temperature [32].

4. Conclusions

We introduce an AM technique based-on electrochemical plating, called the localized pulsed electrodeposition (L-PED) that enables direct printing of nano/micro-pillars of metals and alloys micro-compression test specimens in room environment. The key contribution of L-PED is low cost and high throughput fabrication of small scale test specimens with pristine microstructure and no initial dislocation in one single step in room environment. The L-PED process not only offers precise control over the size of the sample but also allows control over the spatial microstructure of the deposited metal. The proposed method was demonstrated through fabrication and mechanical and electrical testing of nc-nt copper micro-pillars. The microstructure of a selected representative pillar was investigated using high-resolution FIB imaging system. Mechanical properties of the 3D printed micro-pillars were characterized using in situ SEM micro-compression experiment. The printed nc-nt Cu pillars exhibit an average flow stress of 701 \pm 45 MPa at 5% strain. Additionally, electrical properties of the printed nc Cu pillars were investigated in situ SEM. The results showed an average resistivity of $16.14 \pm 3.90~\mu\Omega.cm.$ While the L-PED process as a unique microscale metal AM process can be attractive for various applications where fabrication of complex geometry is needed, its combination with in situ characterization methods can provide high-throughput investigation of the process - microstructure - property relationship for a full understanding of mechanical behavior of metals and metal alloys at smallscale.

Acknowledgment

This work was supported by the US NSF-CMMI (award # 1727539) and the US Office of Naval Research (award # N00014-15-1-2795).

References

- M.F. Pantano, H.D. Espinosa, L. Pagnotta, Mechanical characterization of materials at small length scales, J. Mech. Sci. Technol. 26 (2) (2012) 545–561.
- [2] M.A. Haque, M.T.A. Saif, In-situ tensile testing of nano-scale specimens in SEM and TEM, Exp. Mech. 42 (1) (2002) 123–128.
- [3] M.A. Haque, M.T.A. Saif, A review of MEMS-based microscale and nanoscale tensile and bending testing, Exp. Mech. 43 (3) (2003) 248–255.
- [4] Y. Zhu, N. Moldovan, H.D. Espinosa, A microelectromechanical load sensor for in situ electron and x-ray microscopy tensile testing of nanostructures, Appl. Phys. Lett. 86 (1) (2004), 013506.
- [5] Y. Zhu, A. Corigliano, H.D. Espinosa, A thermal actuator for nanoscale in situ microscopy testing: design and characterization, J. Micromech. Microeng. 16 (2) (2006) 242.
- [6] D. Kiener, C. Motz, T. Schöberl, M. Jenko, G. Dehm, Determination of mechanical properties of copper at the micron scale, Adv. Eng. Mater. 8 (11) (2006) 1119–1125.
- [7] Z.W. Shan, R.K. Mishra, S.A. Syed Asif, O.L. Warren, A.M. Minor, Mechanical annealing and source-limited deformation in submicrometre-diameter Ni crystals, Nat. Mater. 7 (2) (2008) 115–119.
- [8] D.S. Gianola, A. Sedlmayr, R. Monig, C.A. Volkert, R.C. Major, E. Cyrankowski, S. A. Asif, O.L. Warren, O. Kraft, In situ nanomechanical testing in focused ion beam and scanning electron microscopes, Rev. Sci. Instrum. 82 (6) (2011), 063901.
- [9] P.J. Imrich, C. Kirchlechner, D. Kiener, G. Dehm, Internal and external stresses: in situ TEM compression of Cu bicrystals containing a twin boundary, Scr. Mater. 100 (2015) 94–97.
- [10] M.D. Uchic, D.M. Dimiduk, A methodology to investigate size scale effects in crystalline plasticity using uniaxial compression testing, Mater. Sci. Eng. A 400–401 (2005) 268–278.
- [11] H. Zhang, B.E. Schuster, Q. Wei, K.T. Ramesh, The design of accurate microcompression experiments, Scr. Mater. 54 (2) (2006) 181–186.
- [12] J.R. Greer, W.C. Oliver, W.D. Nix, Size dependence of mechanical properties of gold at the micron scale in the absence of strain gradients, Acta Mater. 53 (6) (2005) 1821–1830.
- [13] J.R. Greer, J.-Y. Kim, M.J. Burek, The in-situ mechanical testing of nanoscale single-crystalline nanopillars, JOM (J. Occup. Med.) 61 (12) (2009) 19.
- [14] T. Hirouchi, Y. Shibutani, Mechanical responses of copper bicrystalline micro pillars with Σ3 coherent twin boundaries by uniaxial compression tests, Mater. Trans. 55 (1) (2014) 52–57.

- [15] M.D. Uchic, P.A. Shade, D.M. Dimiduk, Plasticity of micrometer-scale single crystals in compression, Annu. Rev. Mater. Res. 39 (1) (2009) 361–386.
- [16] C.M. Byer, B. Li, B. Cao, K.T. Ramesh, Microcompression of single-crystal magnesium, Scr. Mater. 62 (8) (2010) 536–539.
- [17] A.T. Jennings, J. Li, J.R. Greer, Emergence of strain-rate sensitivity in Cu nanopillars: transition from dislocation multiplication to dislocation nucleation, Acta Mater. 59 (14) (2011) 5627–5637.
- [18] R. Maaß, M.D. Uchic, In-situ characterization of the dislocation-structure evolution in Ni micro-pillars, Acta Mater. 60 (3) (2012) 1027–1037.
- [19] X.W. Gu, C.N. Loynachan, Z. Wu, Y.W. Zhang, D.J. Srolovitz, J.R. Greer, Size-dependent deformation of nanocrystalline Pt nanopillars, Nano Lett. 12 (12) (2012) 6385–6392.
- [20] H. Fei, A. Abraham, N. Chawla, H. Jiang, Evaluation of micro-pillar compression tests for accurate determination of elastic-plastic constitutive relations, J. Appl. Mech. 79 (6) (2012), 061011.
- [21] D. Kiener, C. Motz, M. Rester, M. Jenko, G. Dehm, FIB damage of Cu and possible consequences for miniaturized mechanical tests, Mater. Sci. Eng. A 459 (1–2) (2007) 262–272.
- [22] J.A. El-Awady, C. Woodward, D.M. Dimiduk, N.M. Ghoniem, Effects of focused ion beam induced damage on the plasticity of micropillars, Phys. Rev. B 80 (10) (2009).
- [23] S. Shim, H. Bei, M.K. Miller, G.M. Pharr, E.P. George, Effects of focused ion beam milling on the compressive behavior of directionally solidified micropillars and the nanoindentation response of an electropolished surface, Acta Mater. 57 (2) (2009) 503–510.
- [24] M.J. Burek, J.R. Greer, Fabrication and microstructure control of nanoscale mechanical testing specimens via electron beam lithography and electroplating, Nano Lett. 10 (1) (2010) 69–76.
- [25] A. Behroozfar, S. Daryadel, S.R. Morsali, S. Moreno, M. Baniasadi, A. Bernal Rodrigo, M. Minary-Jolandan, Microscale 3D printing of nanotwinned copper, Adv. Mater. 30 (4) (2017), 1705107.
- [26] S. Daryadel, A. Behroozfar, S.R. Morsali, S. Moreno, M. Baniasadi, J. Bykova, R. A. Bernal, M. Minary-Jolandan, Localized pulsed electrodeposition process for three-dimensional printing of nanotwinned metallic nanostructures, Nano Lett. 18 (1) (2018) 208–214.
- [27] A.J. Bard, L.R. Faulkner, W. John, Sons, Electrochemical Methods: Fundamentals and Applications, John Wiley & Sons, Hoboken, 2007.
- [28] S. Morsali, S. Daryadel, Z. Zhou, A. Behroozfar, D. Qian, M. Minary-Jolandan, Multi-physics simulation of metal printing at micro/nanoscale using meniscusconfined electrodeposition: effect of environmental humidity, J. Appl. Phys. 121 (2) (2017), 024903.

- [29] S. Morsali, S. Daryadel, Z. Zhou, A. Behroozfar, M. Baniasadi, S. Moreno, D. Qian, M. Minary-Jolandan, Multi-physics simulation of metal printing at micro/nanoscale using meniscus-confined electrodeposition: effect of nozzle speed and diameter, J. Appl. Phys. 121 (21) (2017), 214305.
- [30] S. Daryadel, A. Behroozfar, M. Minary-Jolandan, Toward control of microstructure in microscale Additive manufacturing of copper using localized electrodeposition, Adv. Eng. Mater. 0 (0) (2018), 1800946.
- [31] Y. Champion, C. Langlois, S. Guérin-Mailly, P. Langlois, J.-L. Bonnentien, M. J. Hÿtch, Near-perfect elastoplasticity in pure nanocrystalline copper, Science 300 (5617) (2003) 310.
- [32] L. Lu, Y. Shen, X. Chen, L. Qian, K. Lu, Ultrahigh strength and high electrical conductivity in copper, Science 304 (5669) (2004) 422–426.
- [33] D. Jang, C. Cai, J.R. Greer, Influence of homogeneous interfaces on the strength of 500 nm diameter Cu nanopillars, Nano Lett. 11 (4) (2011) 1743–1746.
- [34] D. Jang, X. Li, H. Gao, J.R. Greer, Deformation mechanisms in nanotwinned metal nanopillars, Nat. Nanotechnol. 7 (9) (2012) 594–601.
- [35] M. Mieszala, G. Guillonneau, M. Hasegawa, R. Raghavan, J.M. Wheeler, S. Mischler, J. Michler, L. Philippe, Orientation-dependent mechanical behaviour of electrodeposited copper with nanoscale twins, Nanoscale 8 (35) (2016) 15999–16004.
- [36] X. Zhang, H. Wang, X.H. Chen, L. Lu, K. Lu, R.G. Hoagland, A. Misra, High-strength sputter-deposited Cu foils with preferred orientation of nanoscale growth twins, Appl. Phys. Lett. 88 (17) (2006), 173116.
- [37] M. Dao, L. Lu, Y.F. Shen, S. Suresh, Strength, strain-rate sensitivity and ductility of copper with nanoscale twins, Acta Mater. 54 (20) (2006) 5421–5432.
- [38] L. Lu, X. Chen, X. Huang, K. Lu, Revealing the maximum strength in nanotwinned copper, Science 323 (5914) (2009) 607–610.
- [39] Y.F. Shen, L. Lu, Q.H. Lu, Z.H. Jin, K. Lu, Tensile properties of copper with nanoscale twins, Scr. Mater. 52 (10) (2005) 989–994.
- [40] Z.S. You, L. Lu, K. Lu, Tensile behavior of columnar grained Cu with preferentially oriented nanoscale twins, Acta Mater. 59 (18) (2011) 6927–6937.
- [41] L. Lu, R. Schwaiger, Z.W. Shan, M. Dao, K. Lu, S. Suresh, Nano-sized twins induce high rate sensitivity of flow stress in pure copper, Acta Mater. 53 (7) (2005) 2169–2179.
- [42] I.A. Ovid'ko, A.G. Sheinerman, Mechanical properties of nanotwinned metals: a review, Rev. Adv. Mater. Sci. 44 (2016) 1–25.
- [43] J.C. Ye, Y.M. Wang, T.W. Barbee, A.V. Hamza, Orientation-dependent hardness and strain rate sensitivity in nanotwin copper, Appl. Phys. Lett. 100 (26) (2012), 261912.